Diffusion and drift studies of Ar-DME/CO_2/CH_4 gas mixtures for a radial TPC in the $\mathbf{E} \perp \mathbf{B}$ field

X. Bittl [a], V. Eckardt [a], H. Fessler [a], W.G. Gong [a,1], M. Konrad [a], A. Mock [a], P. Seyboth [a], J.E. Draper [b], M. Hildebrandt [c], K. Ness [d], A. Odian [e], B. Schmidt [c]

[a] *Max-Planck-Institut für Physik, Föhringer Ring 6, D-80805 Munich, Germany*

[b] *Physics Department, University of California, Davis, California, USA*

[c] *Physikalisches Institut der Universität Heidelberg, Philosophenweg 12, D-69120 Heidelberg, Germany*

[d] *Physics Department, James Cook University of North Queensland, Townsville, Queensland 4811, Australia*

[e] *SLAC, Stanford, California, USA*

Abstract

We have performed systematic studies of electron diffusion and drift in three gas mixtures: Ar(50%)-DME(50%), Ar(50%)-CO_2(50%), and Ar(90%)-CH_4(10%) inside the $\mathbf{E} \perp \mathbf{B}$ field, with the aim to build a high-resolution radial Time-Projection-Chamber (TPC). Our TPC design is unconventional in that: (1) it drifts electron clusters in a radial electric field perpendicular to a magnetic field; (2) it employs microstrip gas chamber (MSGC) with pads for readout. To achieve the required spatial resolution and two-track resolution, we find that one must use a gas mixture based on a "cool" gas such as CO_2 or DME (dimethylether $(CH_3)_2O$). Such a gas mixture has low diffusion coefficients and small Lorentz angle in the $\mathbf{E} \perp \mathbf{B}$ field. Its transport parameters are less sensitive to the magnetic field. Our measurements are compared with two transport calculations. For the Ar(90%)-CH_4(10%) gas mixture, the calculations based upon the moments method agree well with our measurements, while the calculations using the Magboltz program largely over-predict our measurements for transverse diffusion and Lorentz angle. For the Ar(50%)-DME(50%) and Ar(50%)-CO_2(50%) gas mixtures, which have slow drift and low diffusion, our measurements are consistent with calculations based upon either the moments method or the Magboltz program.

[1] Corresponding author. E-mail: gong@mppmu.mpg.de

Preprint submitted to Elsevier Science *27 March 1997*

1 Introduction

The Time Projection Chamber (TPC) has become an important detector in many Relativistic Heavy-Ion Collision experiments [1–7]. It has the advantage of tracking charged-particles in three dimensions by using only a two-dimensional readout plus time sampling. Its use of a gaseous medium reduces the probability of multiple scattering and secondary particle productions in a high particle-multiplicity environment. Additionally, multiple sampling of specific ionization gives the capability of particle identification.

The STAR experiment[6] is now being built to search for a new phase of matter (Quark-Gluon-Plasma) using the Relativistic Heavy-Ion Collider (RHIC) at the Brookhaven National Laboratory. A large Time Projection Chamber will be used to track charged particles in the central rapidity region ($|\eta| \leq 1.5$). To cover larger rapidity region ($|\eta|$ up to 4), a forward TPC is proposed. In order to optimize the phase-space acceptance and obtain high spatial and two-track resolution, we adopt a TPC design in which electrons drift in a radial electric field with a perpendicular magnetic field[8–10]. Furthermore, we intend to use the microstrip gas chamber (MSGC) [11–14] for electron amplification and pad readout on a curved surface.

Such a radial TPC design is schematically shown in Fig. 1. The drift cathode, biased at a negative high-voltage, is a tube surrounding the beam pipe. The MSGC readout and front-end electronics are mounted on an outer cylindrical frame. The drift and amplification regions are separated by two cylindrical grids of wires. One is the gating grid, another closer to the MSGC readout is the ground grid. The drift field is established by concentric rings of thin metal tubes on both entrance and exit planes. The voltages on rings are defined by a resistor chain so that a radial field is established.

In a conventional TPC, electrons drift in a uniform electric field parallel to the magnetic field. The magnetic field can reduce the diffusion width transverse to B and E. Pulse heights of electron clusters are amplified in the multi-wire proportional chamber (MWPC) and read out by a two-dimensional pad plane. The Ar(90%)-CH_4(10%) or similar gas mixtures are often used, as they are adequate for many tracking requirements. By adopting the MSGC readout in a TPC design, we expect to improve single-track spatial resolution and two-track resolution considerably. Such resolution requirements are needed to track charged-particles in a high-density region. Additionally, the MSGC gives us the design flexibility in choosing strip geometry and placing the readout plane on a curved surface to maximize the phase-space acceptance. (This would be difficult to do with a wire chamber). Furthermore, we must consider a gas mixture having diffusion coefficients low enough in order to achieve the required spatial resolution and two-track resolution.

Little information was found in the literature on a gas mixture suitable for radial drift in the $\mathbf{E} \perp \mathbf{B}$ field. Initial study of the Ar(90%)-CH_4(10%) gas mixture using the Magboltz program[18] revealed that both the diffusion width and the Lorentz angle were too large to be useful. It was also pointed out[19] that the theoretical treatment in the Magboltz program assumes cylindrical symmetry, which is violated for electron transport in the $\mathbf{E} \perp \mathbf{B}$ field. To improve the situation, we firstly wanted to perform gas measurements inside the perpendicular magnetic field to identify gas mixtures of low diffusion and small Lorentz angles. Secondly, we wanted to test a recent transport program based upon the moments method [20], which is, in principle, suitable for electron transport in an $\mathbf{E} \perp \mathbf{B}$ field. Thirdly, we needed experience in operating a TPC based on the microstrip gas chamber readout to understand any unexpected features related to electron drift and diffusion in a radial $\mathbf{E} \perp \mathbf{B}$ field.

This paper is organized as follows. We first give an introduction to the electron transport calculation based on the moments method in Section 2. To compare calculations with our measurements in a radial $\mathbf{E} \perp \mathbf{B}$ field, we have to treat the cluster-size evolution properly. Such considerations are shown in Section 3. In Section 4, we provide information on the designs of two TPC prototypes, and on the experimental setup. In Section 5, we present our measurements of transport parameters such as transverse/longitudinal diffusion coefficients, drift velocity, and Lorentz angle. We then compared the data to two kinds of calculation: one using the moments method, and the other using the Magboltz program. In Section 6, we comment on the performance of a proposed radial TPC design using the MSGC readout and conclude with a summary.

2 Electron transport program

The information about the drift and diffusion of electrons in a neutral gas is all contained in the electron phase space distribution function f($\mathbf{r}$,$\mathbf{c}$,t). Here, $\mathbf{r}$ denotes the spatial coordinate of an electron at time t, and $\mathbf{c}$ denotes its velocity. The integral of f($\mathbf{r}$,$\mathbf{c}$,t) over $\mathbf{c}$ gives the number density n($\mathbf{r}$,t). This f($\mathbf{r}$,$\mathbf{c}$,t) is found by solving the Boltzmann equation,

$$[\partial_t + \mathbf{c} \cdot \nabla + \frac{e}{m}(\mathbf{E} + \mathbf{c} \times \mathbf{B}) \cdot \partial_c] f(\mathbf{r}, \mathbf{c}, t) = -J f(\mathbf{r}, \mathbf{c}, t) \qquad (1)$$

where ∂_t, ∇, and ∂_c are the gradients with respect to coordinates time t, space $\mathbf{r}$, and velocity $\mathbf{c}$. In the present case, the drift is under the influence of an electric field $\mathbf{E}$ and a magnetic field $\mathbf{B}$, both being uniform, and perpendicular to each other. The terms on the left-hand side of Eq.(1) represent convective flow of the electrons, while the term on the right-hand side represents the effect of collisions and possible reactions between the electrons and the gas molecules. J is the collision operator for the gas mixture[20].

The solution of Eq.(1) is effected by expanding f(**r**,**c**,t) as sums of products with the directional dependence of **c** contained in spherical harmonics $Y_l^{(m)}(\hat{\mathbf{c}})$, the spatial distribution contained in $G_\mu^{(s\lambda)}$, the s-th application of the spatial gradient operator operating on n(**r**,t), and the speed distribution contained in an expansion discussed below. Thus

$$f(\mathbf{r}, \mathbf{c}, t) = \sum_{l=0}^{\infty} \sum_{m=-l}^{l} \sum_{s=0}^{\infty} \sum_{\lambda=0}^{s} \sum_{\mu=-\lambda}^{\lambda} f(lm|s\lambda\mu) Y_l^{(m)}(\hat{\mathbf{c}}) G_\mu^{(s\lambda)} n(\mathbf{r}, t) \tag{2}$$

The coefficients $f(lm|s\lambda\mu)$ are functions of the speed c, obtained by the expansion

$$f(lm|s\lambda\mu) = w(T_b, c) \sum_{\nu=0}^{\infty} F(\nu lm|s\lambda\mu) R_{\nu l}(T_b, c) \tag{3}$$

where $w(T_b, c)$ is a Maxwellian distribution at an adjustable base temperature T_b, and $R_{\nu l}$ is related to a Sonine polynomial (orthogonal set) of order (ν, l). The gas is at the temperature of its drift chamber. The coefficients $F(\nu lm|s\lambda\mu)$ are called "moments", and Eqs.(2) and (3) indicate that they determine f(**r**,**c**,t). These moments are important because they are relatively simply related to the electron transport quantities measured in an experiment, viz., the drift velocity, the Lorentz angle and the matrix of five diffusion coefficients (the other four vanish) that are necessary for this case of perpendicular **E** and **B**. To obtain these measurables, the index s must span the range 0-2 if non-conservative interactions occur, and 0-1 if only conservative interactions occur between the electrons and the neutral gas. The infinite sums must be truncated for a practical solution. Hereafter, we refer calculations based upon this approach as the moments method. For more details, see Ref. [20].

There are two main differences between the solutions obtained with this moments method and the solutions obtained by the Magboltz program[18]. One is that the usual form of the Magboltz program covers only the range in l of 0 to 1, which is not sufficient for good accuracy in many cases. More importantly, the f(**r**,**c**,t) is expanded in terms of Legendre polynomials in the Magboltz program, rather than the spherical harmonics discussed above. The Legendre polynomials (azimuthally symmetric) are sufficient when there is only one reference direction, as when only an electric field is present, or when **E** is parallel to **B**. However, for a gas like $Ar(90\%) - CH_4(10\%)$ where the electron temperature is high and the Lorentz force is strong, the spherical harmonics are needed for the present case of perpendicular **E** and **B**. Of course, this complicates the solution of the Boltzman equation. One can find two recent case studies of the $Ar - CH_4$ gas mixture by comparing calculations based upon the moments method and the Magboltz program [21].

3 Electron transport in the radial $\mathbf{E} \perp \mathbf{B}$ field

In this Section, we define and evaluate parameters related to drift and diffusion in a radial field. A cylindrical coordinate system (r, ϕ, z) is adopted.

An ideal radial electric field is expressed as:

$$|\mathbf{E}(r)| = \frac{V_c}{\ln(R_{out}/R_{in})}\frac{1}{r} \tag{4}$$

where V_c is the voltage on drift cathode, R_{out} and R_{in} are outer and inner radii of the field cage, respectively. The magnetic field is assumed uniform in the z-direction B_z, perpendicular to the electric field E_r.

In a non-uniform drift field, the drift time is

$$T_d = \int_{r_{hit}}^{R_{out}} dt = \int_{r_{hit}}^{R_{out}} \frac{dr}{v_r(r)} \tag{5}$$

Due to the Lorentz force in an $\mathbf{E} \perp \mathbf{B}$ field, the azimuthal deflection angle along the pad-row direction is

$$\Psi_d = \int_{r_{hit}}^{R_{out}} \frac{\psi_L(r)}{r} dr \tag{6}$$

Here, $v_r(r)$ and $\psi_L(r)$ are drift velocity and Lorentz angle at radius r, moving from the hit radius r_{hit} to the readout radius R_{out}.

The electron cluster width in the radial direction evolves according to[9]

$$\sigma_r^2(r + dr) = D_L^2(r) \cdot dr + \sigma_r^2(r) \cdot [1 + \frac{2}{v(r)}\frac{\partial v}{\partial r}dr] \tag{7}$$

The width in the azimuthal direction evolves as[10]

$$\sigma_\phi^2(r + dr) = D_T^2(r) \cdot dr + \sigma_\phi^2(r) \cdot (1 + \frac{dr}{r})^2 \tag{8}$$

D_L is the longitudinal diffusion coefficient along the $\mathbf{E}$ direction. D_T is the transverse diffusion coefficient in the $\mathbf{E} \times \mathbf{B}$ direction. In a radial drift field, D_L and D_T vary as a function of the radius. In addition to the normal diffusion term, the radial width is modified by the drift velocity gradient, and the azimuthal width is modified by the radial divergence.

For simplicity, both the shaper response and pad response are approximated by gaussian distributions. By convoluting the response functions with the respective widths in pad and time directions, we obtain the signal widths as:

$$\sigma_{pad}^2 = \sigma_{prf}^2 + \sigma_\phi^2, \tag{9}$$

$$\sigma_{tim}^2 = \sigma_{shp}^2 + \left[\frac{\sigma_r}{v_r(R_{out})}\right]^2, \tag{10}$$

where $v_r(R_{out})$ is the drift velocity at readout radius, σ_{prf} is the width of pad response function, and FWHM of the shaper $\tau_{shaper} = 2.35\sigma_{shp}$. We remark that for the RTPC, σ_{pad} is calculated differently from Eq.(9) when comparing data and calculations on azimuthal width in Figs. 17(c)-20(c) since the wires are parallel to pads.

To evaluate two-track resolution, we deduce the cluster width at the hit point from the cluster width at the readout plane. In the radial direction,

$$\sigma_r^{hit} = \sigma_{tim} \cdot v_r(r) \tag{11}$$

and in the azimuthal direction,

$$\sigma_\phi^{hit} = \sigma_{pad} \cdot \frac{r}{R_{out}}. \tag{12}$$

The criterion for resolving two close hits is such that their separation must be larger than: $3 \cdot \sigma_r^{hit}$ in the radial direction, or $3 \cdot \sigma_\phi^{hit}$ in the azimuthal direction.

4 Experimental setup and analysis procedure

Two TPC prototypes have been built and used in this work. The first prototype (named micro-STAR) is shown in Fig. 2. It is constructed out of non-organic materials such as stainless steel and ceramics. The chamber is sealed with metallic rings. This way the chamber has minimum outgasing and is compatible with using the DME-based gas mixture[24]. Major components of the micro-STAR are cathode plate, field cage, wire grid, microstrip plate and window ports. The field cage is made of stainless-steel rings, separated by precise ceramic spacers. A resistor chain connects all the rings. One end of the chain is grounded, the other end terminates at the cathode plate which is biased on a negative high voltage. The field cage and cathode plate together establish a uniform drift electric field. The readout is on a double-sided microstrip glass plate, separated from the drift volume by a wire grid. The microstrips are on the front side, and two rectangular pad rows are on the back side. Fig. 3 shows the dimensions and patterns for the anode/cathode-strips (part a) and for the readout pads (part b), respectively. The strips and pads are arranged perpendicularly. The anode width is 8 μm, the cathode width is 400 μm and the pitch is 1 mm. One set of pad has a width of 1.25 mm at a pitch of 1.50 mm, the other has a width of 2.00 mm at a pitch of 2.25 mm. Both pad-lengths are 30.0 mm. The glass plate is 300 μm thick and 10 cm in diameter, mounted on a flange with feed-throughs for readout. The electric connections are made by using flexible Kapton foil with gold traces. The induced charges on the pads are fed into charge-sensitive pre-amplifiers. An electron track is introduced through the gap between two field cage rings, by using either an ultra-violet laser beam or a radioactive source (^{90}Sr). Measurements can be made at two drift distances (d = 5.28, 23.4 cm). This is useful to determine systematic effects in the diffusion measurement and to estimate the magnitude of electron losses during drift. With this chamber, we wanted to study gas properties regarding diffusion and drift in a uniform electric field.

The second TPC prototype (named RTPC) is shown in Fig. 4 with the gas enclosure vessel removed. This chamber was constructed with G-10 and plastic materials, so it is not suitable for measurements using a DME-based gas mixture. Its structure is schematically shown in Fig. 5 . This chamber is special in that it has a radial drift electric field, and all the wire grids and pads are placed on curved planes. It uses the multi-wire proportional chamber for readout, but the sense and field wire grid run parallel to the longer side of a pad. (This construction affects the pad response accordingly.) The sense wires are 20 μm in diameter, placed at 4 mm pitch, while the field wires are placed in the middle between neighboring pair of sense wires. The sense/field wire grid is 4 mm above the pad plane and 4 mm below the ground grid. A gating grid is placed 20 mm further away above the ground grid. A pad has a width of 2.25 mm and a length of 30 mm. Each pad-row has 64 pads placed at a pitch of 2.5 mm. Three pairs of window ports (at drift distance $d = 8, 18, 27cm$) are installed for the UV-laser beam. With this prototype, we wanted to study the particular features associated with diffusion and drift in the radial electric field.

Electron clusters are generated by a UV-laser beam focused into the drift volume. Two types of laser: N_2 and Nd:YAG were used. The N_2 laser emits UV-photons of $\lambda = 337.1$ nm with a nominal pulse-energy of 150 μJ, and pulse width of 0.5 ns. It is adequate for testing the RTPC where high gas gain is obtainable in the multi-wire proportional chamber. The Nd:YAG laser emits IR photons of $\lambda = 1064$ nm; the UV-light of $\lambda = 266$ nm is obtained through a fourth harmonic generator. Its UV-pulse-energy is around 10 mJ. The pulse width is adjustable (2 to 40 ns), the beam spot can be focused to less than 1 mm in diameter. We used this more powerful Nd:YAG laser for testing the micro-STAR where gas gain is limited to 1000-2000 in our microstrip gas chamber.

We use the modified ALEPH TPC readout electronics[15]. The charge-sensitive pre-amplifier is a 16-channel hybrid unit mounted close to the pads. The equivalent noise charge is about 800 electrons at input. The shaper amplifiers and flash ADC's are housed in a FASTBUS crate. The shaper has a shaping time of 180 ns and its output signal is time-sampled at a 12.5 MHz clock frequency. The ADC has a dynamic range of 256 counts. One ADC count is equivalent to about 3900 electron charges. The data acquisition system is based upon the ALEPH Event Builder unit. The trigger is defined by signals from either a photodiode monitoring the laser beam, or a plastic scintillator detecting the transmitted ^{90}Sr β-rays. The data taking is controlled by a PC running Linux.

Two-dimensional ADC pulse height histograms as a function of pad number and time slice are recorded. A peak corresponds to the electron clusters collected over one pad length. In time direction, the peak position with respect to the starting trigger measures the electron drift time which allows to compute the drift velocity. The width of the peak provides information on the longitudinal diffusion coefficient after correcting for the shaper response. In pad direction, the width of the peak provides information on the transverse diffusion coefficient after taking the pad-response-function into consideration. If inside a magnetic field, displacements of the peak position measure the Lorentz angle.

When the cluster width was broad enough to cover more than 3 pads, we normally used a gaussian fit to the pulse-height distribution of pads. However, the cluster width became quite small and often covered only two pads, when we used a cool gas mixture (Ar-DME/CO_2). To measure the cluster accurately, we adopted a scanning procedure. The laser beam was installed on a movable stage and scanned across at least two pad-widths. The scanning step size was 200 to 300 μm. The pulse height distribution was analyzed as a function of the scan position. We used either the distribution of the pulse height on a single pad or the distribution of the pulse-height ratio on two adjacent pads. The one-pad distribution was fitted by a gaussian function. The two-pad ratio distribution was fitted by an error function. Results from both fitting procedures were compared for consistency and combined to assess systematic errors. The pad response was simulated by using the image-charge method from Ref.[16]. It was then convoluted with a given diffusion width to produce the induced pulse-height on pads. A look-up table was obtained for the simulated pulse-height width and the corresponding diffusion width. The diffusion width was thus extracted by matching a measured width with the simulated width. By combining diffusion widths measured at two different drift distances, we obtained the diffusion coefficient (D_T or D_L) at a given field setting.

More information on the experimental setup and the data analysis can be found in Ref.[17].

5 Measurements performed in the $\mathbf{E} \perp \mathbf{B}$ field

We group our measurements into two kinds. The first one deals with questions of gas transport parameters. This kind of measurement was done using the micro-STAR with an uniform electric field and a perpendicular magnetic field. The second one addresses issues related to electron drift and diffusion in a radial electric field and a perpendicular magnetic field. This was done using the radial TPC. Of interest to us are the range of electric field < 1000 V/cm and the nominal magnetic field of 5 kG used in the STAR detector[6]. We made no special corrections for the effects caused by variations in the environmental temperatures and pressures since such effects were minor in the measurements.

5.1 micro-STAR prototype

We performed our measurements at the Max-Planck-Institute for Plasma Physics in Garching, where magnet coils and a power supply were provided. The magnetic field was produced by two groups of Helmholtz coils ($\phi_{in} = 30$ cm) separated by a distance of 42 cm. At the middle point between two coils, the magnitude of magnetic field is about 2.4 G/A. The micro-STAR chamber was positioned around the middle point. The non-uniformity of the magnetic field strength across the sensitive volume is less than 10%, which is adequate for our purpose.

5.1.1 Ar(90%)-CH_4(10%) gas mixture

Fig.6 shows the transverse diffusion coefficient (D_T), measured using the micro-STAR chamber in the $\mathbf{E} \perp \mathbf{B}$ fields. D_T is presented as a function of magnetic field for four representative drift electric fields. We obtained fewer data points at E = 100 V/cm (panel a) than at E = 500 V/cm (panel d) because the Lorentz angles become larger at lower electric fields (see Fig.8) and the electron clusters went outside the pad-rows (see Fig.3(b)). The measured transverse diffusion coefficients (black circle symbols) are larger than 500 μm/$\sqrt{cm}$. They tend to increase at larger magnetic fields. Results of two types of calculations are shown together with data for comparison. One type is based upon the moments method (see Section 2), and shown as open square symbols. The other type uses the Magboltz program [18], and shown as open diamond symbols. Overall our data points are in close agreement with the moments-method calculations. The Magboltz calculations over-predict the D_T data points by as much as 20%. For all calculations the same electron cross sections were used in the Magboltz program and in the moments method. Data on longitudinal diffusion coefficient for P10 had large systematic errors and are not presented here.

Fig.7 shows the drift velocity, as a function of magnetic field at four drift fields (E=100 - 500 V/cm). The drift velocity generally decreases with increasing magnetic field. Results of the two types of calculations are similar, both are in good agreement with our data.

Large sensitivity to the $\mathbf{E} \perp \mathbf{B}$ effect is present in the Lorentz angle, as shown in Fig.8. The measured Lorentz angles increase approximately linearly with the magnetic field. They increase with the magnetic field faster at E = 100V/cm than at E = 500 V/cm. The angle is as big as 20 degrees for E = 500 V/cm and B = 2.5 kG. If a chamber would operate at the nominal STAR magnetic field of 5 kG, the electron cluster would be easily deflected over 50 degrees (according to the calculation). From the point of view of track reconstruction, such a complication is clearly undesirable. The Magboltz program predicts too large Lorentz angles. The calculations based upon the moments method are in closer agreement with the data, although the data lie slightly lower.

To summarize, our measurements are overall in good agreement with the moments-method calculations. The Magboltz calculations clearly show large discrepancies for the transverse diffusion coefficient and Lorentz angle. The Ar(90%)-CH_4(10%) gas mixture has too big transverse diffusion coefficient and Lorentz angle to be suitable for our radial TPC design.

5.1.2 Ar(50%)-DME(50%) gas mixture

To look for a suitable gas, we studied the Ar(50%)-DME(50%) gas mixture. DME is a well-known cool gas after it was first studied for a high-resolution drift chamber[22]. This gas has the following interesting features: (1) low drift velocity and very low diffusion coefficient ($\sim$ 60 μm/$\sqrt{cm}$)[22]; (2) better quenching property by absorbing UV-photons of wavelength $<$ 200 nm [23]; (3) slow aging rate for radiation exposure up to 1 C/cm if a chamber uses stainless steel or gold-plated wires and uses properly selected construction and tubing materials [24]. But in the past it had problems with Freon-11 impurity (as low as 0.1 ppm) and with most plastic materials, and even with two types of resistive wires made of Ni or Cr[24]. Our micro-STAR chamber was designed and constructed according to suggestions found in the literature, and avoided problematic materials.

Fig.9 shows the transverse diffusion coefficients as a function of the drift field. Panel (a) is for no magnetic field; panel (b) is for a perpendicular magnetic field of B = 4.8 kG. One sees that the transverse diffusion coefficients are around 100 μm/$\sqrt{cm}$ for E $>$ 400 V/cm and increase to 200 μm/$\sqrt{cm}$ at E $\approx$ 100 V/cm. There appears to be little dependence on the magnetic field. The data points shown as black circle symbols are measured with the laser-scanning procedure at two drift distances. (The analysis procedure was outlined in Section 4.) The points displayed by star symbols are measured at the longer drift distance only by centering a 3-pad distribution on the middle pad. The width information was extracted from the ratios of pulse heights between mid-pad and side-pads. The star symbols lie slightly lower than the black circle symbols, this difference therefore reflects our systematic error. The calculation based on the moments method is as much as 30% larger than the calculation based on the Magboltz program for E $<$ 300 V/cm. But because of large systematic errors, our data can not distinguish between the two calculations.

Fig.10 shows the longitudinal diffusion coefficients as a function of E for (a) B = 0 and (b) B = 4.8 kG respectively. The data points are measured with the laser-scanning procedure at two drift distances. Again, they are insensitive to the magnetic field and are consistent with both calculations shown in the figure. Together with Fig.9, one sees that the electron cloud diffuses rather isotropically.

Fig.11 shows the drift velocity as a function of E for (a) B = 0 and (b) B = 4.8 kG, respectively. The drift of electrons is very slow. The drift velocity is approximately proportional to E with a slope of 6×10^{-4} [cm/μs]/[V/cm]. The drift velocity has small dependence on the magnetic field. The data points are in good agreement with the moments-method calculations. The Magboltz calculations are about 10% below the measured values.

The Lorentz angles are presented as a function of drift field E for a fixed B = 4.8 kG in Fig.12(a), and as a function of magnetic field B for a fixed E = 500 V/cm in Fig.12(b), respectively. The Lorentz angles at all E fields are as small as 2 degrees. The data points are again in agreement with the moments-method calculations, the Magboltz calculations are about 10% smaller than the moments-method calculations. The angle increases linearly with the magnetic field as expected.

To summarize, we found that both the transverse and longitudinal diffusion coefficients are around 100 μm/$\sqrt{cm}$, the Lorentz angle is only 2 degrees, nearly independent of the electric field. For a "cool" gas mixture, the perpendicular magnetic field has almost negligible effect. The difference between the two types of calculations is around 10%. Our measurement, especially of the drift velocity and Lorentz angle, favors the moments-method calculations.

5.1.3 Ar(50%)-CO_2(50%) gas mixture

Considering the extra precautions required for handling the DME gas, we have studied an alternative gas mixture – Ar(50%)-CO_2(50%). CO_2 is another known cool gas, but non-flammable and more conventional. Although the diffusion coefficient of pure CO_2 is about 20 μm/$\sqrt{cm}$ larger than that of pure DME for E/p > 1500 V/cm, the diffusion coefficients of both gases are comparable for E/p < 700 V/cm[22].

For the Ar(50%)-CO_2(50%) gas mixture in the $\mathbf{E} \perp \mathbf{B}$ fields, both measurements and calculations for the transverse diffusion coefficient, the longitudinal diffusion coefficient, the drift velocity, and the Lorentz angle are shown in Figs.13 to 16, respectively. Because the pad-row assembly in the micro-STAR is not wide enough, most of the measurements were made at B = 2.4 kG, less than half of our nominal magnetic field (5 kG). We point out that data points for the longitudinal diffusion coefficient were not shown because they had too large uncertainty. Overall, our data are in good agreement with both types of calculations. The difference between the two types of calculations is rather small. This gas mixture shows little sensitivity to the $\mathbf{E} \perp \mathbf{B}$ effect. In comparison, the Lorentz angle of the CO_2-mixture is about 4 degrees at B = 5 kG, twice as large as that of the DME-mixture; the drift velocity of the CO_2-mixture is also twice as big as that of the DME-mixture. The diffusion coefficients of both mixtures are small and comparable.

5.2 RTPC prototype

Having obtained transport parameters of 3 gas mixtures in the uniform $\mathbf{E} \perp \mathbf{B}$ fields, we proceeded to study the radial TPC (RTPC) prototype. The purpose is to understand the special feature of drifting an electron cluster in a radial electric field and a perpendicular magnetic field. Since the radial TPC prototype was not compatible with the DME-mixture, we only studied the other two gas mixtures of Ar(50%)-CO_2(50%) and Ar(90%)-CH_4(10%).

Our measurements were performed in the West Area of CERN where a large magnet was available. The volume of the magnetic field is 3.72 $\times$ 1.22 $\times$ 0.8 m^3. The maximum field strength is 7.5 kG. The radial TPC (see Fig.4) was positioned in the middle of the magnet. Using the N_2 UV-laser, we measured the clusters drifting over three different distances at various settings of drift voltage (V_c) and magnetic field (B). For the sake of comparison, the vertical scales in Figs.17 - 20 are all kept identical except panel (a) for the drift time.

5.2.1 Ar(50%)-CO_2(50%) gas mixture

In Fig.17, we present measurements of cluster parameters as a function of drift distance. The RTPC chamber was operated at a drift voltage of 15 kV and a perpendicular magnetic field of 5 kG. Because the cluster drifts in a non-uniform electric field, we can not compare the transport parameters with calculations in a direct way. Instead, we compare a cluster parameter measured at the readout radius with the same parameter calculated by propagating the cluster through the non-uniform field to the readout radius. Transport parameters from the moments-method (or the Magboltz program) calculations are used here as inputs. The black circle points show measured parameters such as drift time (μs), deflection angle (degree), azimuthal width (mm), and radial width (μs) in the figure panel (a) to (d) respectively. The definition of those parameters and the cluster propagation through the radial field is explained in Section 3.

One sees that the total drift time reaches 60 μs and the deflection angle is less than 5 degrees for a drift distance of 30 cm at V_c = 15 kV. Two calculations by the moments method (open square symbols) and by the Magboltz program (open diamond symbols) are hardly distinguishable for drift time, deflection angle and azimuthal angle. But in Fig.17(d), the measurement of the radial width is in closer agreement with the calculations by the moments method. Since the diffusion width in the CO_2 mixture is not much larger than the sense-wire pitch (4 mm), the azimuthal widths are dominated by the pad response function and have weak dependence on drift distance in panel (c). In contrast, the radial widths in panel (d) are dominated by the diffusion width (shown in terms of μs) and have a strong dependence on drift distance.

Because the drift velocity does not saturate in our operational range of electric field, the radial cluster width can be significantly affected, as expressed in the last term of Eq.(7) in Section 3. To see the magnitude of this effect, we made another calculation (without this velocity-gradient term) using transport parameters by the moments method, as shown by open triangle symbols in panel (d). The large difference between open symbols and triangle symbols clearly underlines the importance of this velocity-gradient term.

In Fig.18, we present the cluster parameters as a function of the magnetic field for a fixed drift distance (d = 27 cm). The drift time, azimuthal and radial widths have almost no dependence on the magnetic field up to 7.5 kG. It is reassuring that the perpendicular magnetic field has a minimum effect on drift velocity and diffusion width if such a cool gas mixture as Ar(50%)-CO_2(50%) is used. One expects that the Ar(50%)-DME(50%) gas mixture would behave similarly.

5.2.2 Ar(90%)-CH_4(10%) gas mixture

The Ar(90%)-CH_4(10%) mixture is a fast gas, it is affected more by the $\mathbf{E} \perp \mathbf{B}$ field. For this gas mixture, we present measurements of cluster parameters as a function of drift distance in Fig.19, and as a function of magnetic field in Fig.20, respectively. The RTPC chamber was operated at a drift voltage of 7.5 kV and a perpendicular magnetic field of *only* 0.5 kG. The magnetic field was limited to such a low value by the pad-row assembly because of the large Lorentz angle for the P10 gas. For a drift distance of 30 cm, the total drift time is 6μs, but the total deflection angle is as large as 12 degrees. One sees that the moments-method calculation gives a much better prediction for the deflection angle in panel (b), but the differences in total drift time and cluster widths between two calculations are very small.

In panel (d), the radial width in terms of μsec shows a weak dependence upon the drift distance. This doesn't imply the diffusion width is small. Rather it is due to the large shaper time (σ_{shp} = 76.6 ns) and the fast drift speed of this gas mixture. In panel (c), the strong dependence upon drift distance is consistent with the large transverse diffusion coefficient (see Fig.6). The actual discrepancy of 0.5 mm between data points and calculations is not well understood, it may have something to do with the pad-response function when the wires are parallel to the pads. This feature is not desirable, but had to be adopted due to the difficulty in stretching wires on a curved surface.

In Fig.20 (a) and (d), we observe that the measured total drift time and radial width have some dependence upon the magnetic field up to 1 kG. As mentioned earlier, we cannot increase the magnetic field higher at a drift distance of 18 cm. If the RTPC were to operate at the nominal magnetic field of 5 kG with P10, the total deflection angle would be over 50 degrees.

To summarize, we find that the Ar(50%)-CO_2(50%) gas mixture is a good choice for operating a radial TPC in the $\mathbf{E} \perp \mathbf{B}$ field. The total deflection angle and cluster widths are small, and the total drift time is acceptable. We note that there exist special features associated with diffusion in a radial field, for example, the velocity-gradient term in Eq.(7) and the $\frac{1}{r}$-divergent term in Eq.(8). From Figs.17(c) and 19(b) we conclude that the transport parameters for drift and diffusion in the $\mathbf{E} \perp \mathbf{B}$ field are better reproduced by the moments method than by the Magboltz program.

6 Discussion and conclusion

From the results obtained so far, we want to evaluate the performance of a radial TPC design as sketched in Fig.1. This TPC has inner and outer radii of 8 cm and 32 cm, respectively. Its length is 120 cm, with 10 planes of microstrip-pad readout. Every pad is 2 cm long. The drift voltage is set at 10 kV, and the chamber operates at a perpendicular magnetic field of 5 kG. The Ar(50%)-CO_2(50%) gas mixture is used.

We assume that a cluster is generated (at Z = 210 cm) by a primary track originating from the collision vertex (at Z = 0). Fig.21 shows , as a function of the hit radius (where a cluster originates), the cluster parameters of total drift time (T_d in μs), total deflection angle (Ψ_d in degree), single cluster width in pad direction (σ_{pad} in mm) and in time direction(σ_{tim} in μs), and two-track resolution (two clusters separated by 3σ) in radial direction(σ_r in mm) and in azimuthal direction(σ_ϕ in mm). In panel (a), the maximum drift time is less than 50 μs. In panel (b), the maximum deflection angle is less than 6 degrees. In panel (c), the maximum cluster width in pad direction is 1.2 mm, and in time direction is 300 ns. The rise of σ_{tim} with increasing r is due to the dip angle of a track along the pad. In panel (d), the two-track resolutions at r = 8 cm (where the particle track density is high) are 7 mm in radial direction, and 1 mm in azimuthal direction, respectively. These performance parameters are expected to meet the physics requirement of tracking charged-particles in the pseudo-rapidity range ($|\eta| \approx$ 2-4) at RHIC.

To conclude, we have studied three gas mixtures of Ar(50%) - DME(50%), Ar(50%) - CO_2(50%), and Ar(90%) - CH_4(10%) inside the $\mathbf{E} \perp \mathbf{B}$ fields using the micro-STAR and the radial TPC prototypes. We found that transport parameters predicted by the moments method are generally in better agreement with our measurements, than predictions by the Magboltz program. A gas mixture containing cool gases such as DME or CO_2 has small diffusion coefficients and a small Lorentz angle, and it shows small sensitivity to the $\mathbf{E} \perp \mathbf{B}$ effect. Within the context of the STAR experiment, our design of a new radial TPC with microstrip readout is expected to meet the required spatial and two-track resolutions in the large rapidity region, when the gas mixture of Ar(50%)-CO_2(50%) is used.

7 Acknowledgement

We wish to thank the Technical Division of the Max-Planck-Institute for Physics for their excellent and efficient support in building the micro-STAR chamber. We acknowledge that the radial TPC chamber was originally built at the Brookhaven National Laboratory and University of California, Davis and later modified at the Max-Planck-Institute for its test. Discussions with Dr. K. Foley are appreciated. We greatly appreciate the assistance provided by Dr. H. Lohnert and his colleagues in arranging and operating the magnet setup at the Max-Planck-Institute for Plasma Physics. We are grateful to Mr. D. Hauff and his colleagues at the Semiconductor Laboratory of the Max-Planck-Institute for their valuable work in fabricating microstrip plates. This work is partially supported by the RHIC STAR Detector R&D contract No. 776729.

References

[1] J.W. Harris et al., Nucl. Instr. and Meth. **A315** (1992) 33.

[2] A. Kuehmichel and NA49 Collaboration, Nucl. Instr. and Meth. **A360** (1995) 30.

[3] M.D. Partlan et al., Phys. Rev. Lett. **75** (1995) 2100.

[4] S.E. Eiseman et al., Phys. Lett. **B297** (1992) 44.

[5] E. Andersen et al., Phys. Lett. **B327** (1994) 433.

[6] J.W. Harris et al., Nucl. Phys. **A566** (1994) 277c.

[7] J. Schukraft et al., Nucl. Phys. **A566** (1994) 311c.

[8] J.E. Draper, STAR Note* **45** (1992) and STAR Note **211** (1995); J.E. Draper, D. Cebra, J.L. Romero, STAR Note **172** (1994); J.E. Draper, L. Wood, J.L. Romero, D. Cebra, F.P. Brady, STAR Note **187** (1995).

[9] M. Konrad, STAR Note **214** (1995).

[10] F.P. Brady and J.L. Romero, Nucl. Instr. and Meth. **A333** (1993) 312.

[11] A. Oed, Nucl. Instr. and Meth. **A263** (1988)351.

[12] T.M.V. Bootsma et al., Nucl. Instr. and Meth. **A349** (1994) 204.

[13] W.G. Gong, H. Wieman, J.W. Harris, J.T. Mitchell, W.S. Hong, V. Perez-Mendez, IEEE Trans. Nucl. Sci. **V41:N4** (1994)890.

[14] V. Eckardt, H. Fessler, M. Konrad, S. Krisch, Proc. Int'l Workshop on Micro-Strip Gas Chambers, Legnaro, Oct. 1994, page 184.

[15] W.B. Atwood et al., Nucl. Instr. and Meth. **A306** (1991) 446.

[16] W. Blum and L. Rolandi, Particle Detection with Drift Chambers, Springer-Verlag, 1993.

[17] X. Bittl, Diploma Thesis, Max-Planck-Institute for Physics, 1997.

[18] S.F. Biagi, Nucl. Instr. and Meth. **A283** (1989) 716.

[19] S.F. Biagi and J.E. Draper, private communications.

[20] K.F. Ness, Phys. Rev. **E47** (1993) 327; K.F. Ness, Austr. J. Phys. **48** (1995) 557.

[21] R.E. Robson, M. Hildebrandt, B. Schmidt, preprint, Univ. of Heidelberg, (1997); J.E. Draper and K.F. Ness, preprint, Univ. of California, Davis, (1997).

[22] F. Villa, Nucl. Instr. and Meth. **217** (1983) 273.

[23] M. Jibaly et al., Nucl. Instr. and Meth. **A273** (1988)161.

[24] M. Jibaly et al., Nucl. Instr. and Meth. **A283** (1989)692.

---

* STAR Note is an internal technical publication of the STAR experiment at the Brookhaven National Laboratory. It is accessible at: URL = http://rsgi01.rhic.bnl.gov/star/starlib/doc/www/star.html.

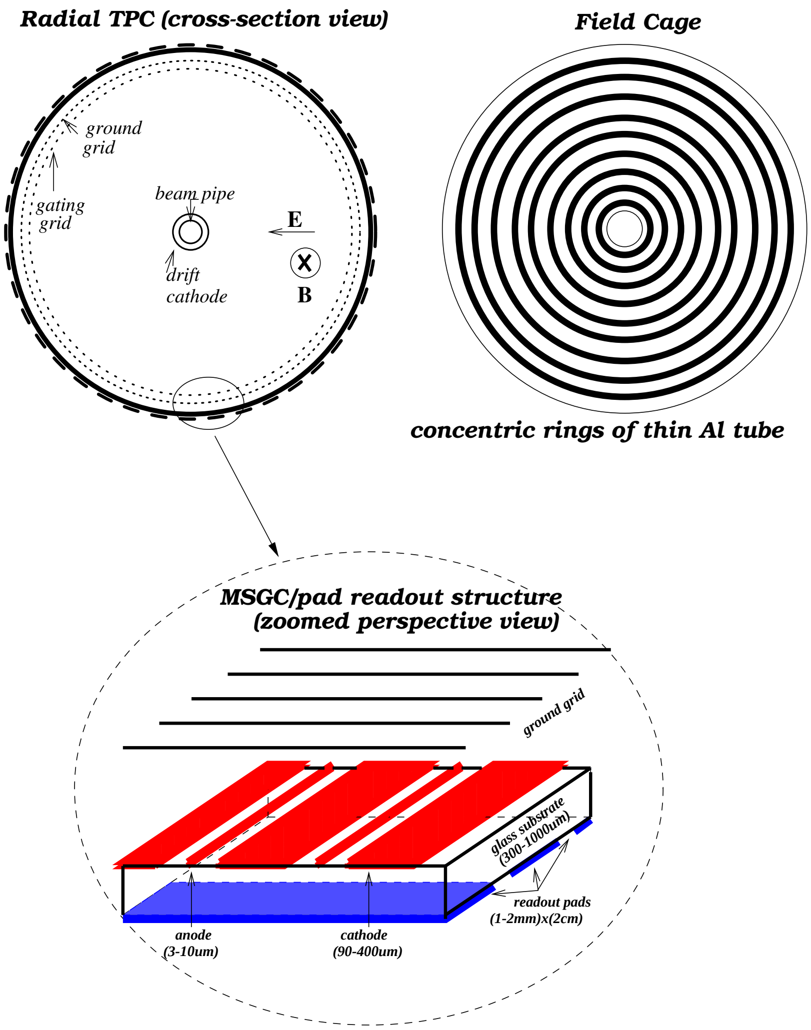

Fig. 1. A schematic view of the radial TPC design with the MSGC-pad readout.

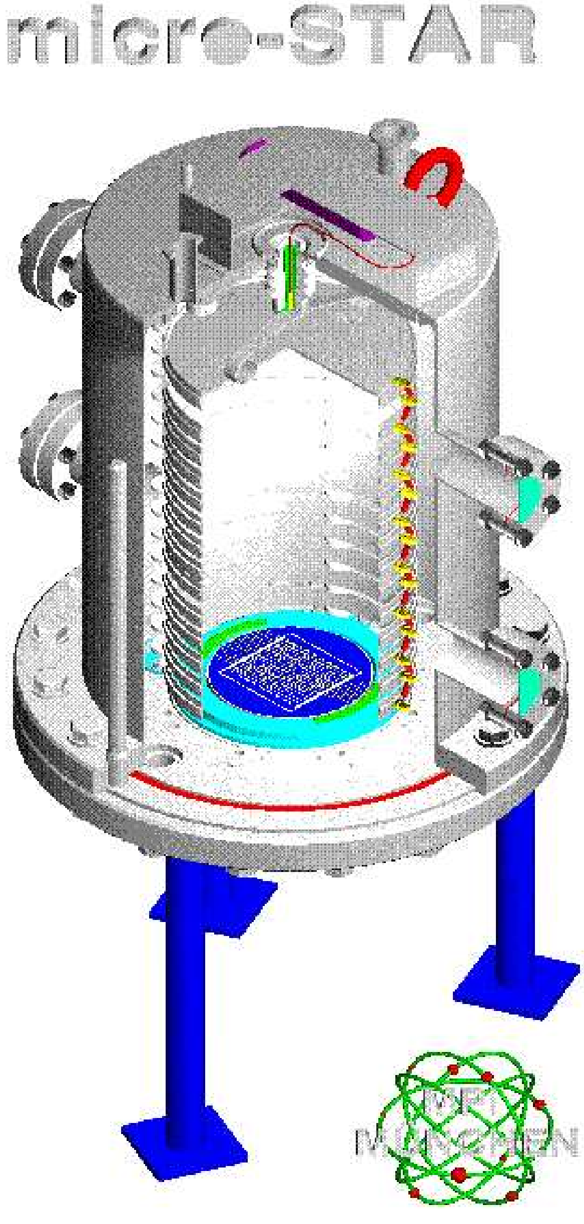

Fig. 2. Picture of the micro-STAR chamber with its inner structure exposed. This chamber is built out of non-organic materials such as stainless steel and ceramics.

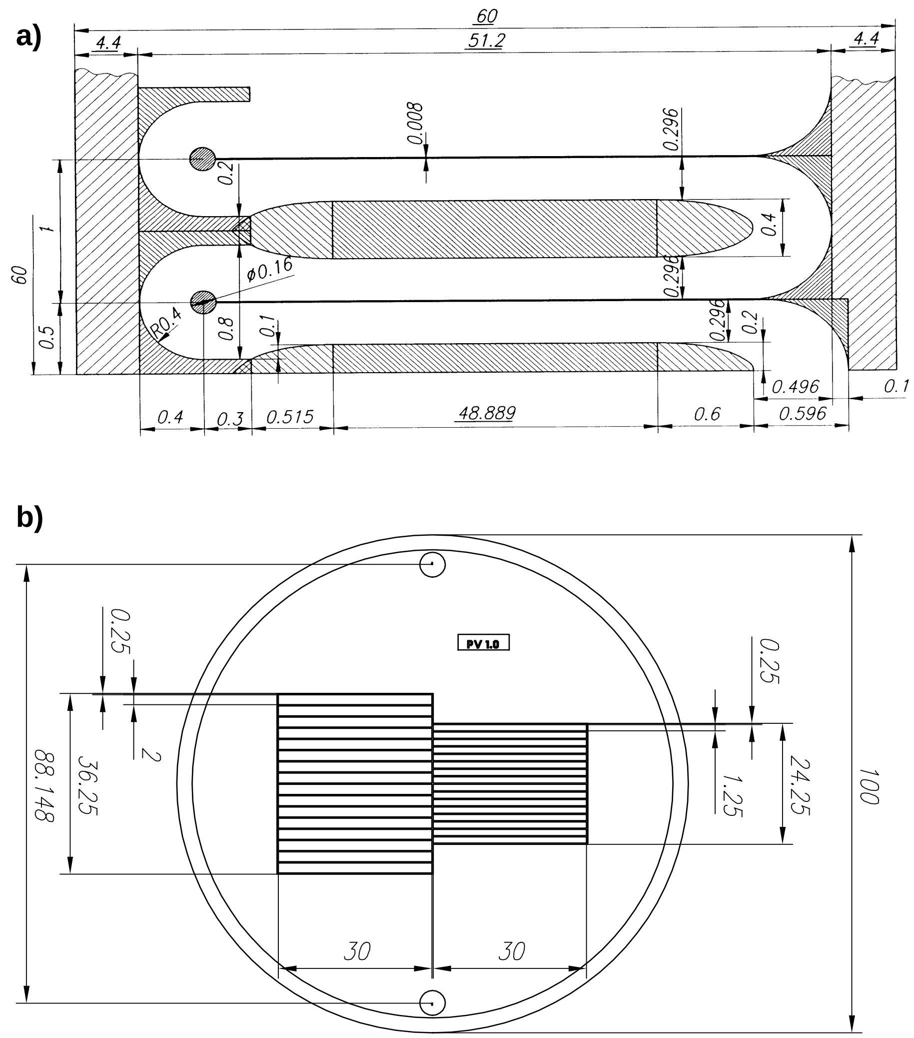

Fig. 3. Design of a double-sided microstrip glass plate. (a) front-side: anode- and cathode-strips for electron amplification (60 mm long at 1 mm pitch); (b) back-side: pads to read out the induced signal (2 rows of different pad-widths shown). The anode/cathode strips are arranged perpendicularly to the pads.

Fig. 4. Picture of the radial TPC prototype with the gas enclosure vessel removed.

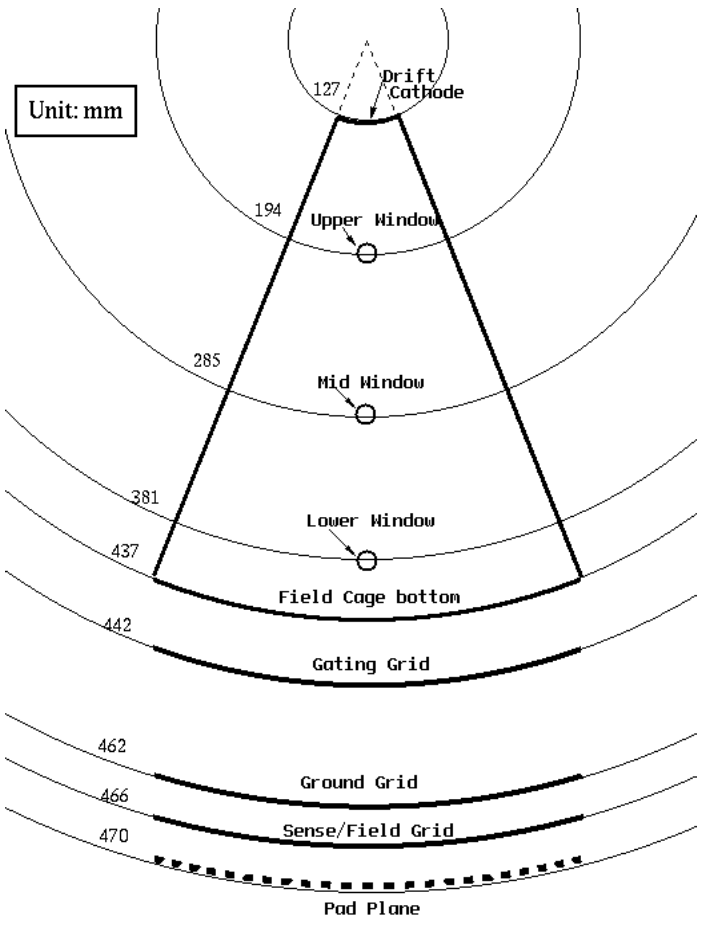

Fig. 5. Schematic diagram of the RTPC prototype with the MWPC readout. The pad-rows are on the curved surface and the wires are stretched parallel to the pads.

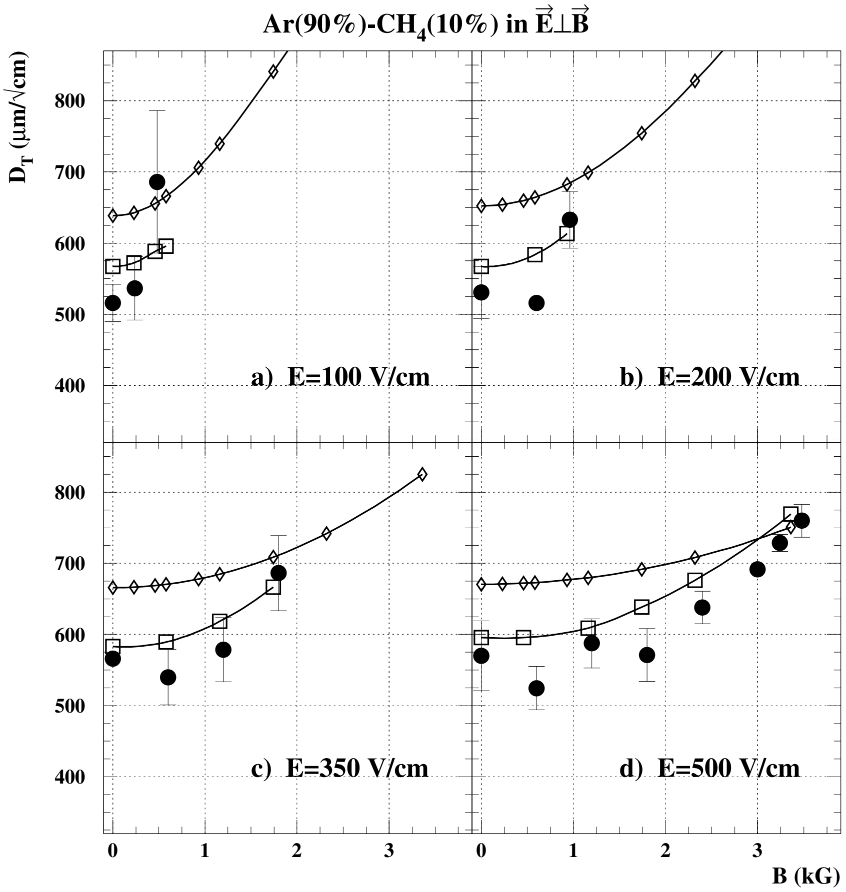

Fig. 6. Transverse diffusion coefficient of the Ar(90%)-CH_4(10%) gas mixture as a function of the magnetic field at four drift fields: (a) E=100 V/cm; (b) E=200 V/cm; (c) E=350 V/cm; (d) E=500 V/cm. The plots show data points (•), calculations using the moments method (□), and calculations using the Magboltz program (◇); smooth curves were drawn to connect the results of the calculations.

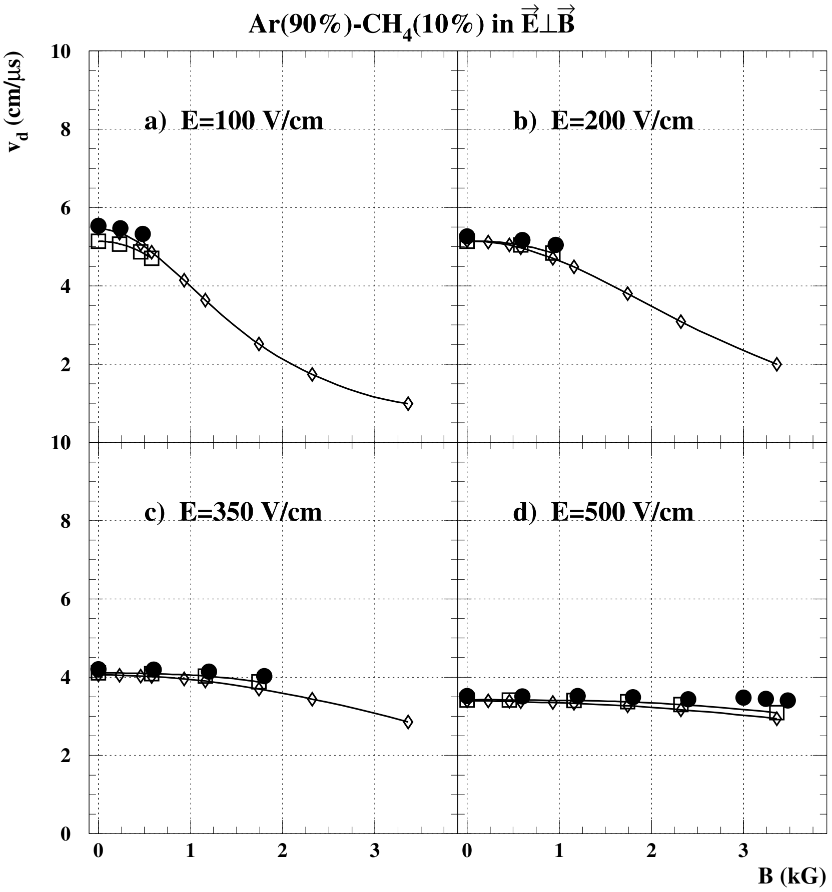

Fig. 7. Drift velocities of the Ar(90%)-CH_4(10%) gas mixture as a function of the magnetic field at four drift fields: (a) E=100 V/cm; (b) E=200 V/cm; (c) E=350 V/cm; (d) E=500 V/cm. The plots show data points (•), calculations using the moments method (□), and calculations using the Magboltz program (◇); smooth curves were drawn to connect the results of the calculations.

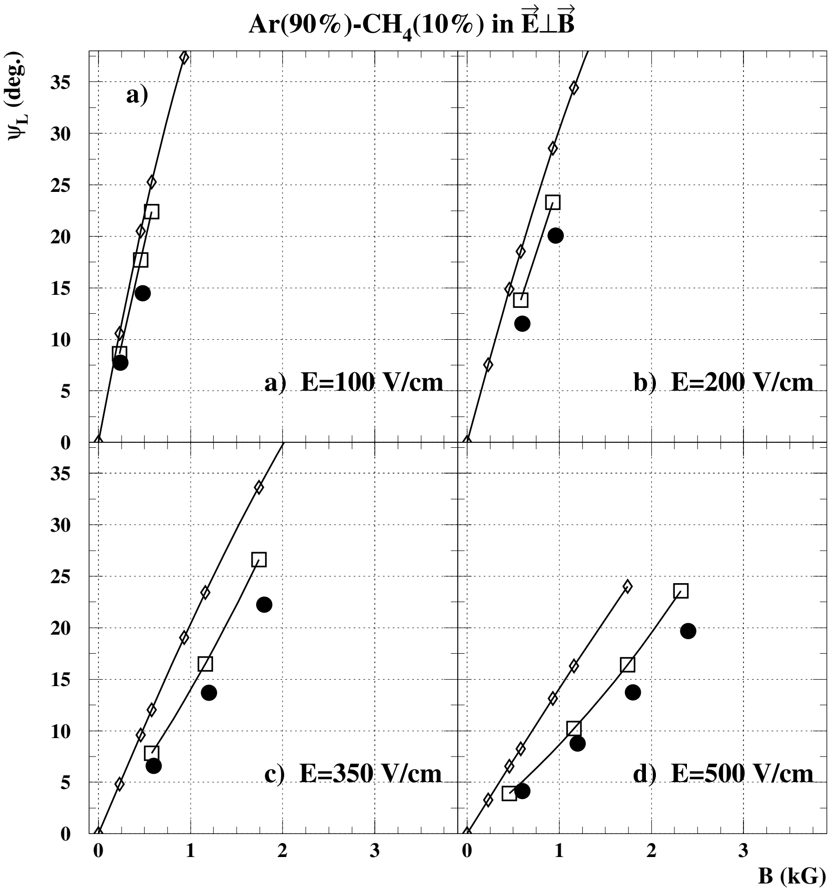

Fig. 8. Lorentz angles of the Ar(90%)-CH_4(10%) gas mixture as a function of the magnetic field at four drift fields: (a) E=100 V/cm; (b) E=200 V/cm; (c) E=350 V/cm; (d) E=500 V/cm. The plots show data points (•), calculations using the moments method (□), and calculations using the Magboltz program (◇); smooth curves were drawn to connect the results of the calculations. Experimental uncertainties are smaller than the points.

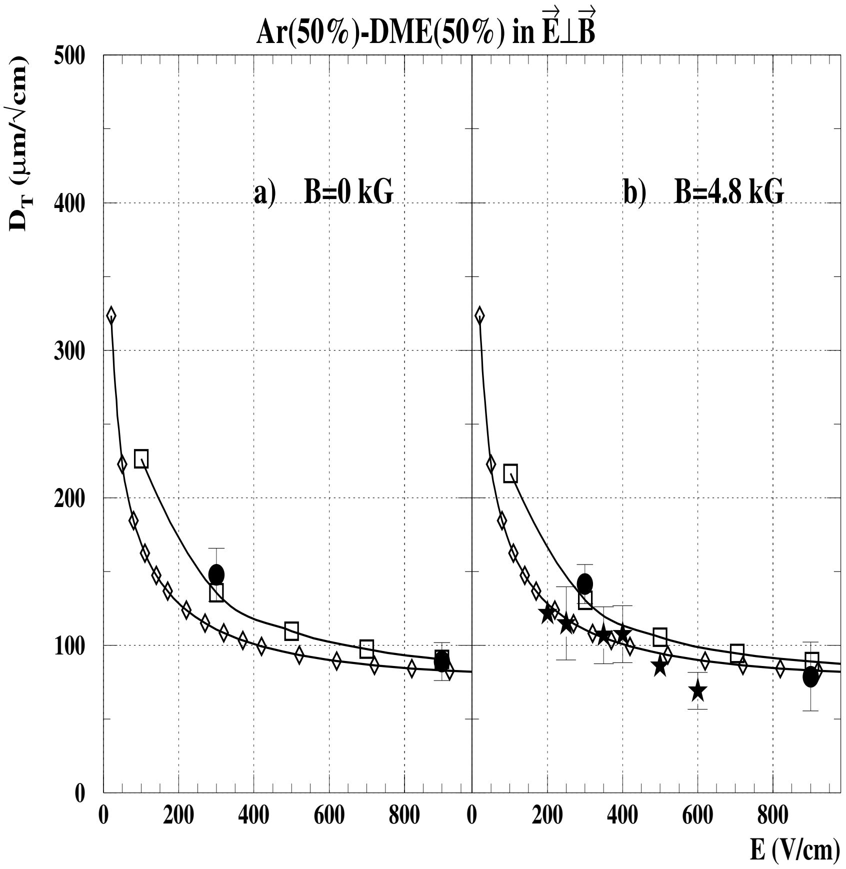

Fig. 9. Transverse diffusion coefficient of the Ar(50%)-DME(50%) gas mixture as a function of the drift field for : (a) B=0 kG; (b) B=4.8 kG. The plots show data points ($\bullet, \star$), calculations using the moments method ($\Box$), and calculations using the Magboltz program ($\Diamond$); smooth curves were drawn to connect the results of the calculations.

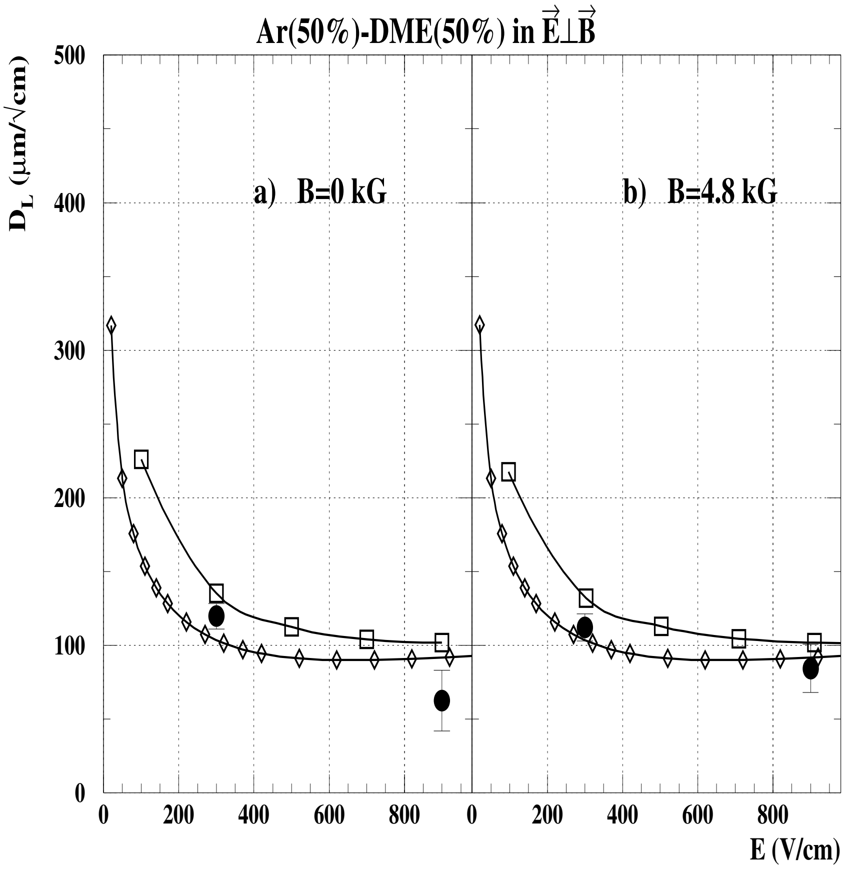

Fig. 10. Longitudinal diffusion coefficient of the Ar(50%)-DME(50%) gas mixture as a function of the drift field for : (a) B=0 kG; (b) B=4.8 kG. The plots show data points (●), calculations using the moments method (□), and calculations using the Magboltz program (◇); smooth curves were drawn to connect the results of the calculations.

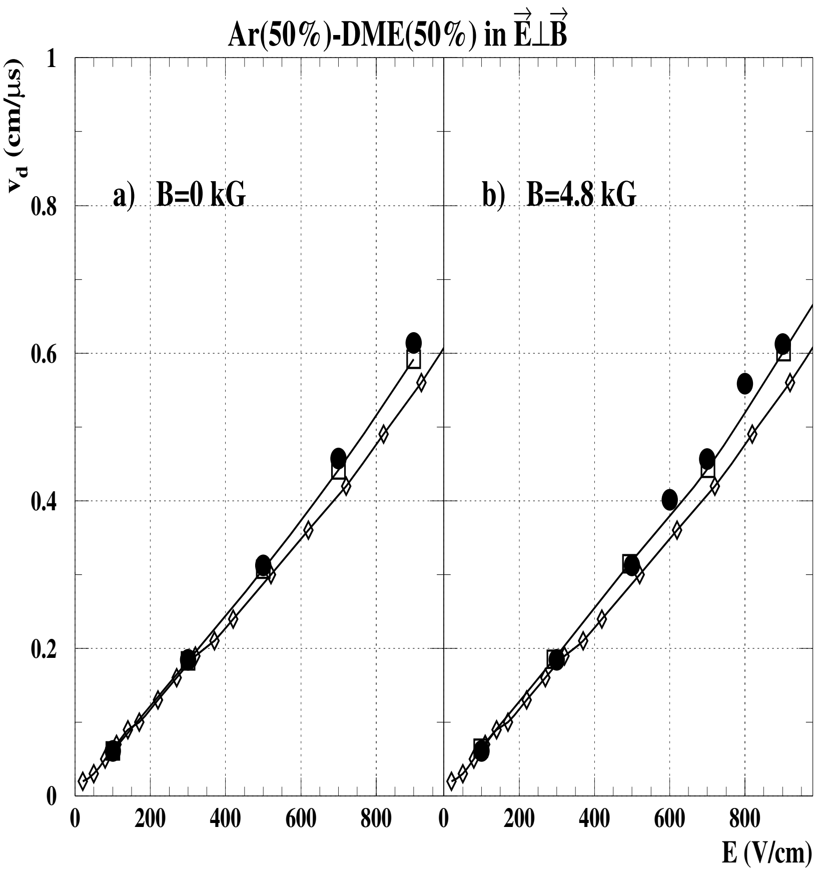

Fig. 11. Drift velocities of the Ar(50%)-DME(50%) gas mixture as a function of the drift field for : (a) B=0 kG; (b) B=4.8 kG. The plots show data points (•), calculations using the moments method (□), and calculations using the Magboltz program (◇); smooth curves were drawn to connect the results of the calculations.

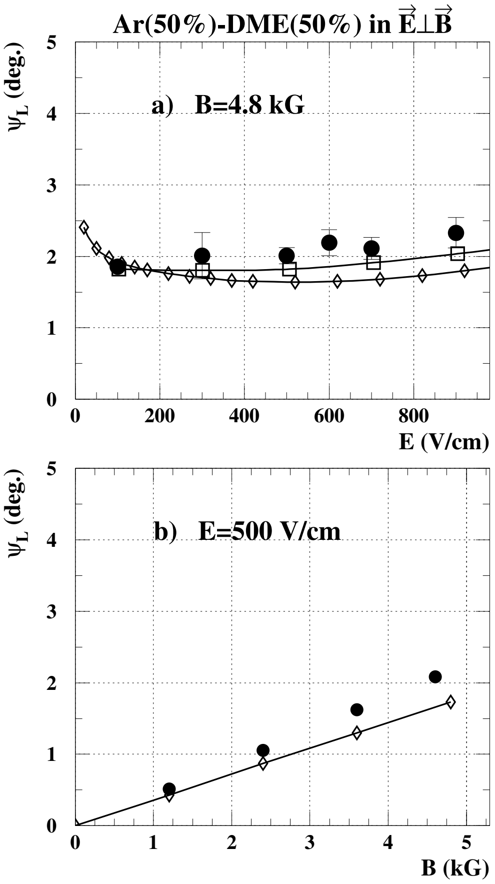

Fig. 12. Lorentz angles of the Ar(50%)-DME(50%) gas mixture: (a) as a function of the drift field for B=4.8 kG; (b) as a function of the magnetic field for E=500 V/cm. The plots show data points (•), calculations using the moments method (□), and calculations using the Magboltz program (◇); smooth curves were drawn to connect the results of the calculations.

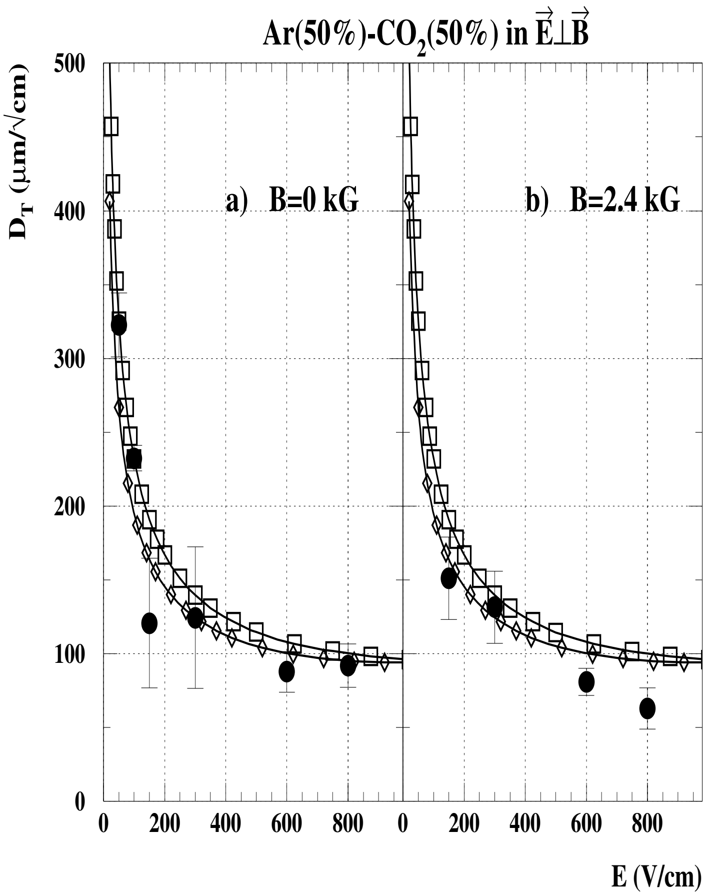

Fig. 13. Transverse diffusion coefficient of the Ar(50%)-CO_2(50%) gas mixture as a function of the drift field for : (a) B=0 kG; (b) B=2.4 kG. The plots show data points (•), calculations using the moments method (□), and calculations using the Magboltz program (◇); smooth curves were drawn to connect the results of the calculations.

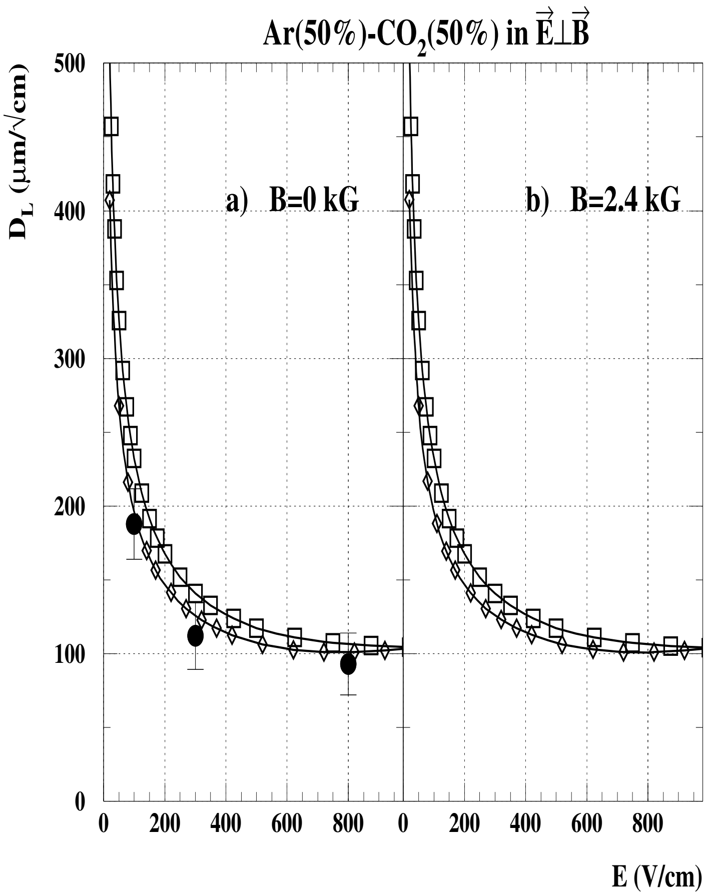

Fig. 14. Longitudinal diffusion coefficient of the Ar(50%)-CO_2(50%) gas mixture as a function of the drift field for (a) B=0 kG; (b) B = 2.4 kG. The plots show data points (●), calculations using the moments method (□), and calculations using the Magboltz program (◇); smooth curves were drawn to connect the results of the calculations.

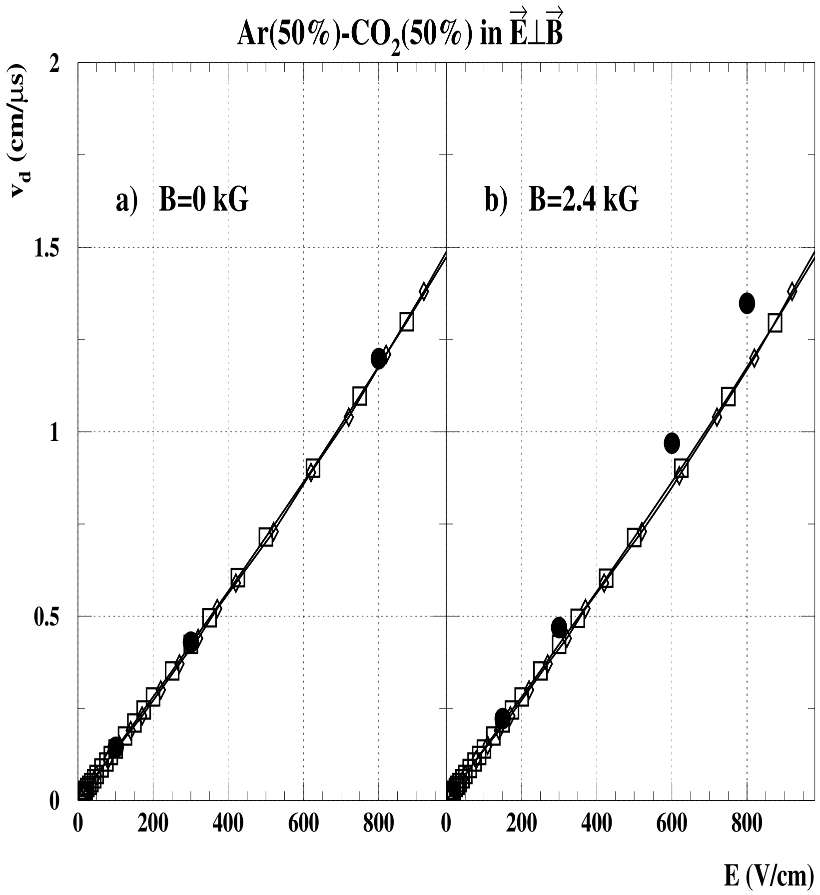

Fig. 15. Drift velocities of the Ar(50%)-CO_2(50%) gas mixture as a function of the drift field for : (a) B=0 kG; (b) B=2.4 kG. The plots show data points (•), calculations using the moments method (□), and calculations using the Magboltz program (◇); smooth curves were drawn to connect the results of the calculations.

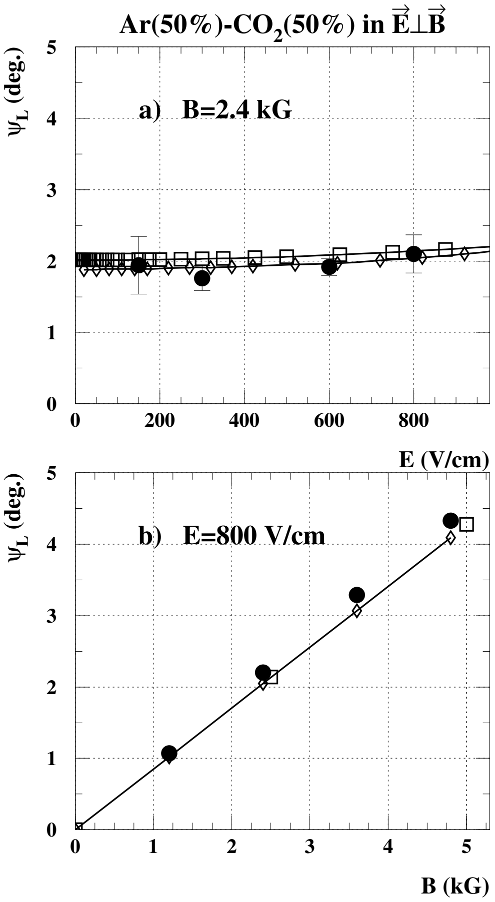

Fig. 16. Lorentz angles of the Ar(50%)-CO_2(50%) gas mixture: (a) as a function of the drift field for B=2.4 kG; (b) as a function of the magnetic field for E=800 V/cm. The plots show data points (•), calculations using the moments method (□), and calculations using the Magboltz program (◇); smooth curves were drawn to connect the results of the calculations.

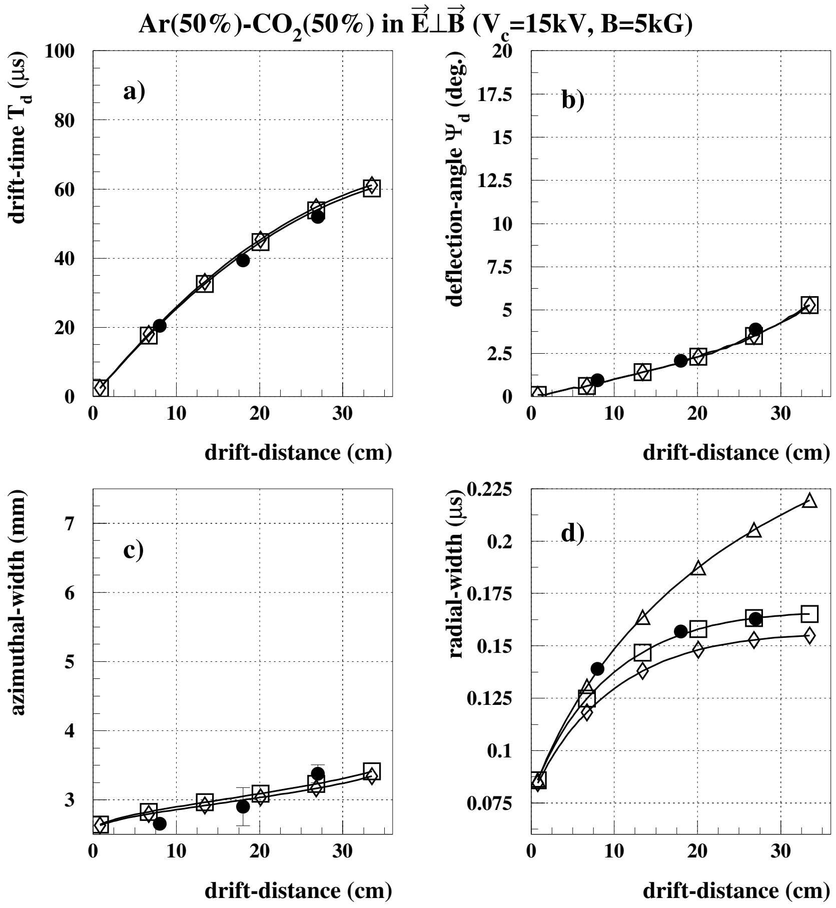

Fig. 17. Electron cluster parameters of the Ar(50%)-CO_2(50%) gas mixture as a function of the drift distance inside the RTPC prototype: (a) drift time (μs); (b) deflection angle (degree); (c) azimuthal cluster width (mm); and (d) radial cluster width (μs). The plots show data points ($\bullet$), calculations using the moments method ($\square$ with and $\triangle$ without the $\frac{\partial v}{\partial r}$ term in Eq. 7), and calculations using the Magboltz program ($\diamond$); smooth curves were drawn to connect the results of the calculations.

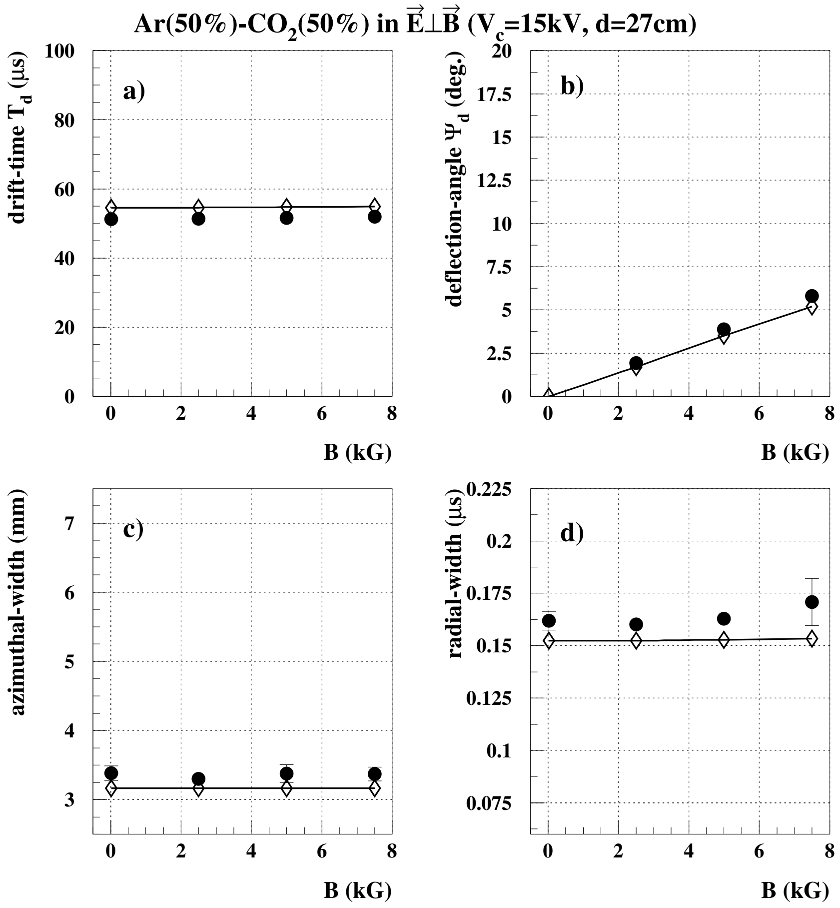

Fig. 18. Electron cluster parameters of the Ar(50%)-CO_2(50%) gas mixture as a function of the magnetic field inside the RTPC prototype: (a) drift time (μs); (b) deflection angle (degree); (c) azimuthal cluster width (mm); and (d) radial cluster width (μs). The plots show measured data points ($\bullet$), and calculations using the Magboltz program ($\diamond$); smooth curves were drawn to connect the results of the calculations.

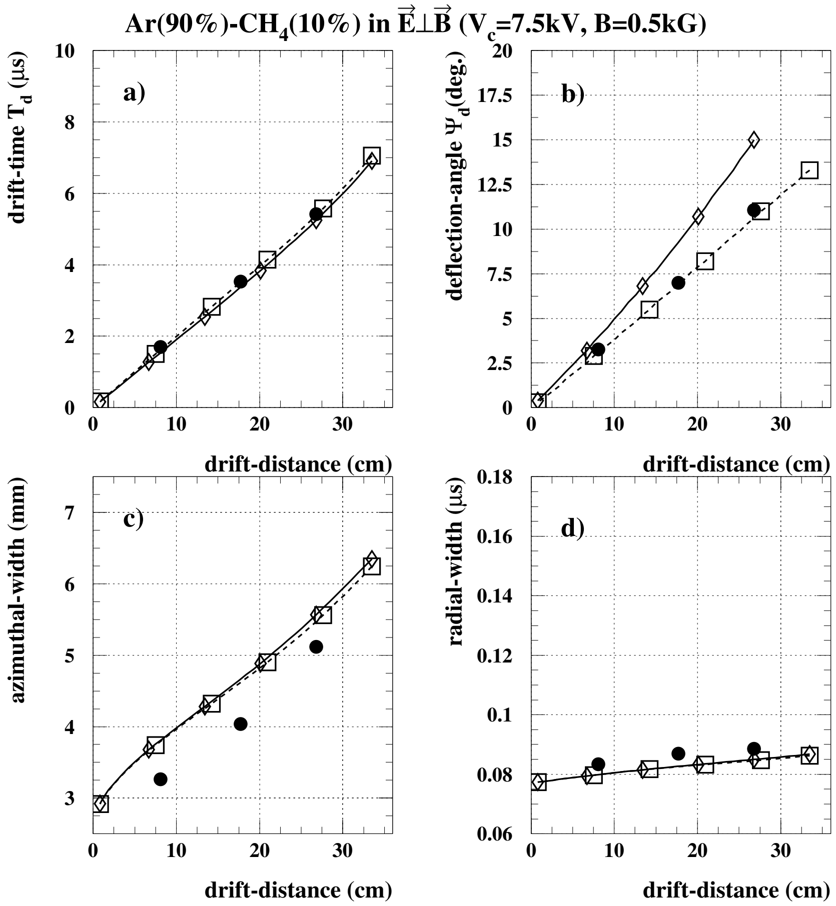

Fig. 19. Electron cluster parameters of the Ar(90%)-CH_4(10%) gas mixture as a function of the drift distance inside the RTPC prototype: (a) drift time (μs); (b) deflection angle (degree); (c) azimuthal cluster width (mm); and (d) radial cluster width (μs). The plots show measured data points ($\bullet$), calculations using the moments method ($\square$), and calculations using the Magboltz program ($\diamond$); smooth curves were drawn to connect the results of the calculations.

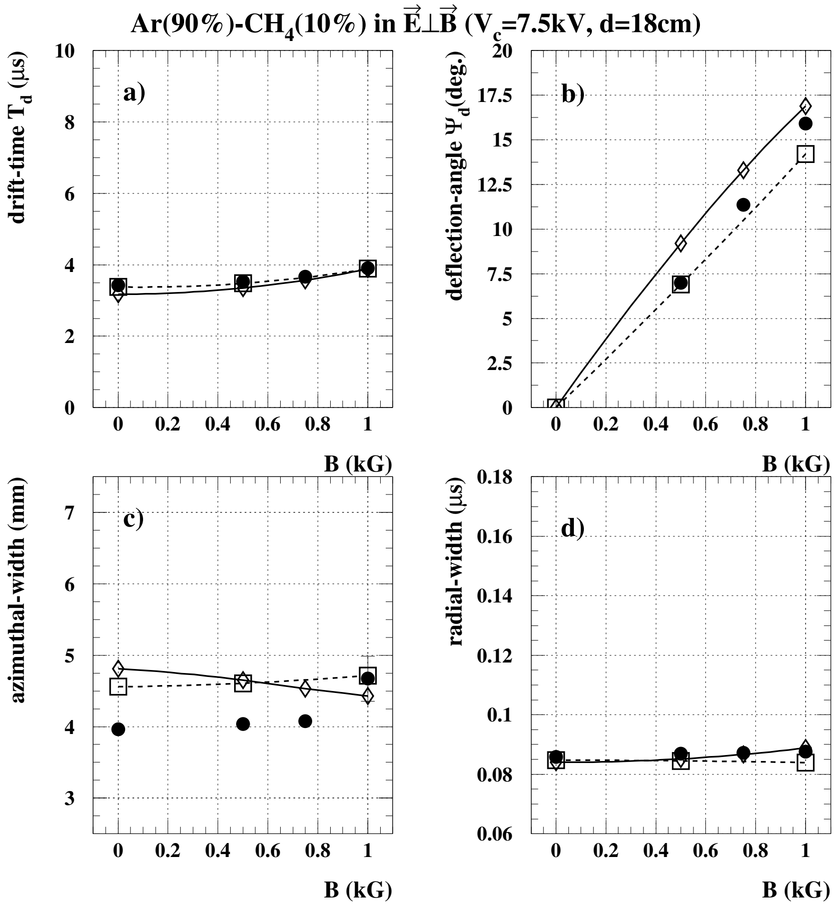

Fig. 20. Electron cluster parameters of the Ar(90%)-CH_4(10%) gas mixture as a function of the magnetic field inside the RTPC prototype: (a) drift time (μs); (b) deflection angle (degree); (c) azimuthal cluster width (mm); and (d) radial cluster width (μs). The plots show measured data points ($\bullet$), calculations using the moments method ($\square$), and calculations using the Magboltz program ($\diamond$); smooth curves were drawn to connect the results of the calculations.

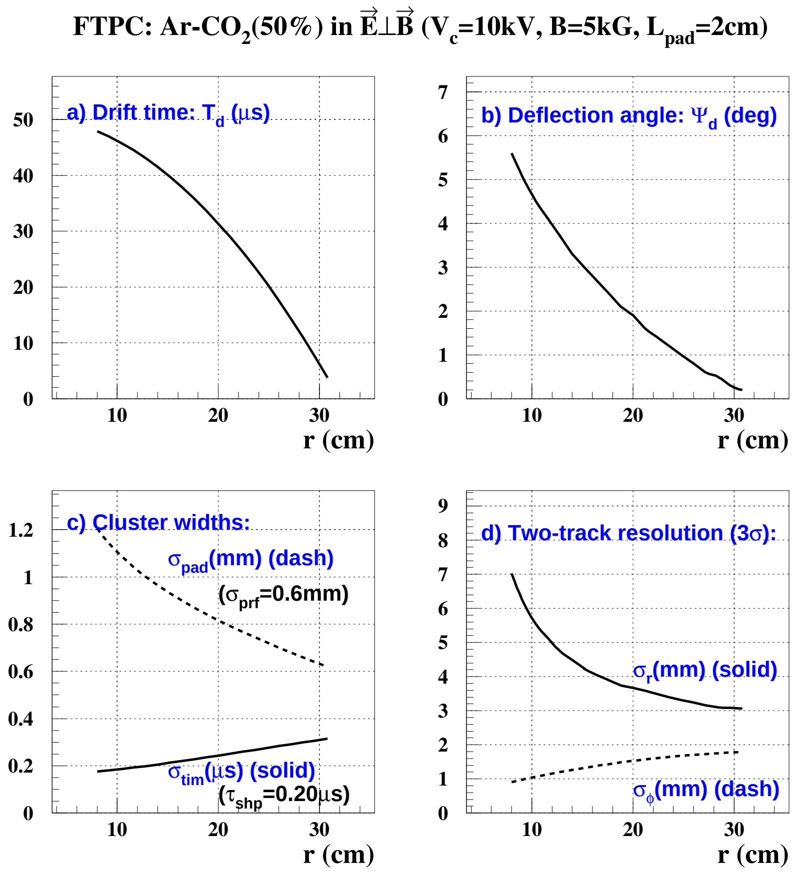

Fig. 21. Electron cluster parameters as a function of the hit radius for a radial TPC design using the Ar(50%)-CO_2(50%) gas mixture. (a) drift time; (b) deflection angle; (c) cluster widths in time direction (solid line in μsec) and in pad direction (dashed line in mm); (d) two-track resolution (by 3σ) in the radial direction (solid line) and in the azimuthal direction (dashed line).